*Proc. Natl. Acad. Sci. USA*
Vol. 96, pp. 6700–6704, June 1999
Biophysics

# Nonlinear optical measurement of membrane potential around single molecules at selected cellular sites

GADI PELEG*†, AARON LEWIS*‡, MICHAL LINIAL§, AND LESLIE M. LOEW¶

*Division of Applied Physics, Center for Neural Computation, Department of Ophthalmology, Hadassah Laser Center, and §Department of Biological Chemistry, Life Science Institute, Hebrew University of Jerusalem, Jerusalem 91904, Israel; and ¶Department of Physiology, University of Connecticut Health Center, Farmington, CT 06030-1507

*Communicated by Y. Ron Shen, University of California, Berkeley, CA, March 1, 1999 (received for review August 20, 1998)*

**ABSTRACT** **Membrane potential around single molecules has been measured by using the nonlinear optical phenomenon of second harmonic generation. This advance results from the interaction between a highly dipolar molecule with a selectively directed highly polarizable 1-nm gold particle. With this approach, a second harmonic signal, which is enhanced by the nanoparticle, is detected from a volume of nanometric dimensions. This present work clearly shows that functional cellular imaging around single molecules is possible by selectively directing an antibody with a 1-nm gold label to a specific membrane protein. The results of this work open the way for three-dimensional, high resolution functional imaging of membrane electrophysiology in cells and cellular networks.**

Recently, it has been shown that the nonlinear optical phenomenon of second harmonic generation (SHG) is a sensitive monitor of cellular membrane potential (1, 2). To observe SHG with sensitivities comparable to linear optical phenomena, tightly focused pulsed laser light with high peak power is required. As reviewed by Nie and Zare (3) single molecules were successfully observed in linear optical imaging as early as 1981 and most recently, with great success, by using confocal microscopy to limit the out-of-focus light that severely degrades the signal to noise in linear optical imaging. However, SHG, either in an imaging or a nonimaging mode, has not been accomplished with single molecule sensitivity.

SHG arises from the second term of the expansion of the molecular electron polarizability shown below and thus is called a second-order nonlinear optical phenomenon.

$$P = \chi^{(1)} * E + \chi^{(2)} * E * E + \chi^{(3)} * E * E * E + \ldots$$

where P is the polarization, E is the applied optical electric field, and $\chi^{(n)}$ are the $n$th order optical susceptibilities. In the recent past, the third term of this equation has generated a lot of interest in biological imaging because it is responsible for the nonlinear optical phenomenon of two-photon fluorescence (TPF) (4–8). The use of nonlinear optics results in naturally high $x, y$, and $z$ spatial resolution, and, in general with nonlinear optical microscopy, photodamage and photobleaching are reduced because the out-of-focus light does not result in excitation. However, for the particular case of SHG, no photochemistry occurs even in the focal plane because the signal, stimulated by nonresonant radiation, does not involve an excited state with a finite lifetime. Optical effects arising from the first term (linear processes) and the third terms of this equation have no fundamental restriction on the symmetric distribution of the dye molecules that give rise to these phenomena in the cells. Second harmonic generation, on the other hand, has a requirement that symmetrically distributed chromophores will not contribute to the observed signal. This symmetry restriction results in a considerable advantage to the nonlinear optical imaging of cell membranes and their membrane potential because only those molecules that are asymmetrically distributed in the cell membrane contribute to the observed signal. The actual membrane potential sensitivity of the second harmonic intensity has been discussed previously (1, 2). In brief, the second harmonic intensity is related, in the final analysis, to the dipole induced in the dye molecule by the electromagnetic field of the light, and this induced dipole is altered by the potential across the membrane.

To approach SHG with single molecule sensitivities, we adapt an old idea that has been applied to the linear optical phenomenon of Raman scattering. In Raman scattering, it has been shown that the presence of a roughened silver surface has the ability to achieve significant enhancement of molecules by a process that is known as surface-enhanced Raman scattering (9). Such roughened silver surfaces also have been applied to the enhancement of nonlinear optical phenomena (10, 11). Theoretically, it can be shown that the close association with silvered nanostructured regions that exist on such roughened surfaces should in fact have an even larger effect on nonlinear optical phenomena if these regions are closer to an elliptical structure (12). In spite of this, such roughened silver surfaces are difficult to apply to the problem we would like to address in this paper, which concerns the selective enhancement of nonlinear optical phenomena in nanometric regions of biological systems.

To realize the enhancement that can be achieved with nanometrically structured metal particles, we used a metal nanoparticle complexed to an antibody that can be directed to specific sites in a cell membrane by standard methods that have been used in electron microscopy. The metal particles that we have used are composed of gold rather than silver. These particles also can effectively enhance such optical phenomena because gold, like silver, possess surface plasmon states that are involved in the enhancement phenomenon. In this way, we are able to direct the particle to a region of a cell membrane that has been labeled with a chiral, highly dipolar, styryl membrane anchoring dye, JPW 1259 (see Fig. 1 for a diagrammatic representation). This dye, which generates large signals, has been shown (1, 2) to be selectively detectable in cell membranes at a concentration (≈1% of total lipids) that is similar to what is used in linear fluorescence imaging of cells stained with such dyes. This observation, along with the present work, is based on the realization, in earlier investigations (13–16), that the SHG from molecules with large induced

The publication costs of this article were defrayed in part by page charge payment. This article must therefore be hereby marked "*advertisement*" in accordance with 18 U.S.C. §1734 solely to indicate this fact.

PNAS is available online at www.pnas.org.

Abbreviations: SHG, second harmonic generation; TPF, two-photon fluorescence.

‡To whom reprint requests should be addressed at: Division of Applied Physics, Bergmann Building, Hebrew University of Jerusalem, Jerusalem 91904, Israel. e-mail: lewisu@vms.huji.ac.Il.
†Present address: Chemistry Department, Stanford University, Stanford, CA 94305-5080.

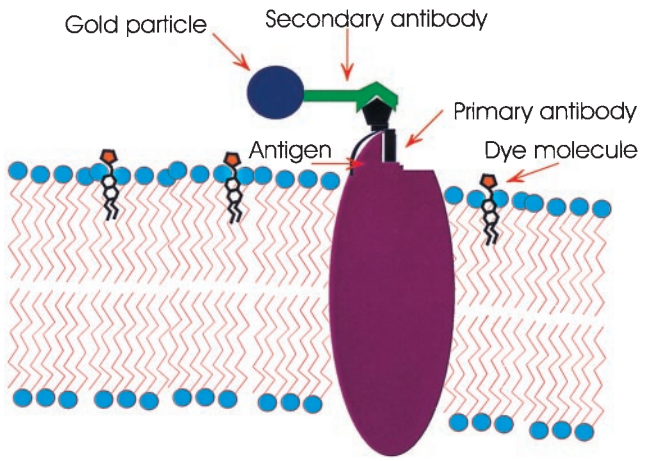


FIG. 1. Diagramatic representation of the relationship of dye molecules bound to the lipid bilayer and nanometric gold particles bound to an antigenic site on the membrane.

dipoles can be selectively detected in times reasonable for imaging at biologically relevant concentrations. This is the case even though they may constitute a small natural or artificially embedded component in a membrane or membrane protein.

## METHODS

**The Cells.** Undifferentiated P19 neuronal cells were grown on microscope coverslips according to previously published procedures (17) and were maintained during the nonlinear optical measurements in a medium that was composed of 116.1 mM NaCl, 5.4 mM KCl, 2 mM $CaCl_2$, 2 mM $MgCl_2$, 25 mM Hepes, 30 mM glucose, and 0.05% BSA at a pH of 7.4. High KCl solution was composed of 31.5 mM NaCl, 90 mM KCl, 2 mM $CaCl_2$, 2 mM $MgCl_2$, 25 mM Hepes, 30 mM glucose, and 0.05% BSA at a pH of 7.4. The cells were stained with JPW1259 (1, 2) by using the filtered physiological buffer. The resulting solution had an optical density of not more than 0.4 at 466 nm. To prepare this final solution, the dye first was dissolved in 0.25% DMSO, 0.25% ethanol, and 0.05% pluronic F127 (Sigma).

**The Nonlinear Optical Microscope.** The optical system used in these experiments of simultaneous second harmonic and two-photon nonlinear optical studies has been described elsewhere (18). For these imaging experiments, the sample was placed on a standard coverslip that fits into a unique three-dimensional piezo-driven flatscanning stage from Nanonics Imaging (Jerusalem). This compact scanner, which is 7 mm thick and has a central clear aperture, can be scanned in $x$ and $y$ with a rough resolution of 1 $\mu$ over several millimeters and has fine resolution capability over 70 $\mu$ of less than an angstrom. It also has the capability of $z$ extensions with the same fine resolution of up to 70 $\mu$.

The laser used was a 1.064 $\mu$ Q-Switched–Mode-Locked Nd:YAG laser. The Q-switched frequency was 400 Hz, and the mode-locked pulse duration was 80–100 ps. The beam was transmitted through a polarizer and a half wave plate for intensity and polarization control. A photodiode provided the means to monitor the near infrared intensity. A filter was placed in front of the entrance port of the microscope to prevent any second harmonic intensity that was created by the optical elements from entering the microscope.

The laser light was focused with a 0.5 numerical aperture/ $\times$50 long working distance objective lens of the inverted microscope (Zeiss, IM 35) onto the sample, and the nonlinear optical signal generated in the sample was collected with lenses held in the condenser track above the sample stage and was detected through an H10 ISA (1,200 lines/mm grating, 2-mm slits, 100-mm focal length) monochromator (Instruments SA, Metuchen, New Jersey) to measure the wavelength of the effects we observed. The fundamental intensity was blocked from entering the monochromator by a filter of $OD_{7.0}$ at 1.064 $\mu$.

The SHG or TPF intensity was detected by a photomultiplier (model R1477, Hamamatsu, Tokyo) and was amplified ($\times$25), averaged, and integrated by a boxcar averager/channel integrator (Stanford Research, Palo Alto, CA). These signals were transferred to a computer in which the images were generated. In most of the experiments described in this work, the average laser power at the cells was 4–5 mW. The recording time corresponded to 30 ms/pixel in a 64 $\times$ 64 image. Images were processed with NIH IMAGE 1.54 (National Institutes of Health) by applying a X3 smoothing filter and a pseudocolor look-up table.

**Gold-Conjugated Antibodies.** The primary antibody used was against stage-specific embryonic antigen 1 and was produced by using a previously reported procedure (19). The gold-conjugated secondary antibody was purchased from British BioCell International (Cardiff, U.K.). These antibodies were goat anti-mouse IgG. The undifferentiated P19 neuronal cells were incubated for $\approx$2 hours with the primary antibody for stage-specific embryonic antigen 1 and then were washed three times. The cells remained in the growth medium for 10 min after each wash. The cells then were incubated for 1.5 hours with the secondary antibody. Finally, a triple wash was performed again. The last step was to change the medium to an optically transparent physiological medium as described above in the subsection, above, on "The Cells." In each coverslip, the concentrations of the primary and secondary antibodies were determined according to previous electron microscopic studies that have defined the protocol for specific densities of gold balls on the cell membrane. Controls were run in each set of experiments by skipping the stage of primary antibody incubation and to check the role of each ingredient in the labeling system.

**Acidic Wash Assay.** To verify experimentally the existence of the 1-nm gold particles in the images, we performed an acidic wash assay. In this assay, a wash protocol was performed between taking successive nonlinear optical images to disrupt the bond connecting the particles to the membrane by a procedure that had been devised previously (20). We verified that the procedure of acid washing did not alter the membrane potential of the cells by using the second harmonic signal as our monitor.

## RESULTS AND DISCUSSION

SHG and TPF images of JPW1259-stained cells are shown in Fig. 2. These images typify the patterns of these nonlinear optical signals seen in cells stained with this chiral potential-sensitive dye. In the right of Fig. 2*A* appear the membranes of two cells that have been stained with the dye. In addition, a third cell is within this field of view in the upper left. This

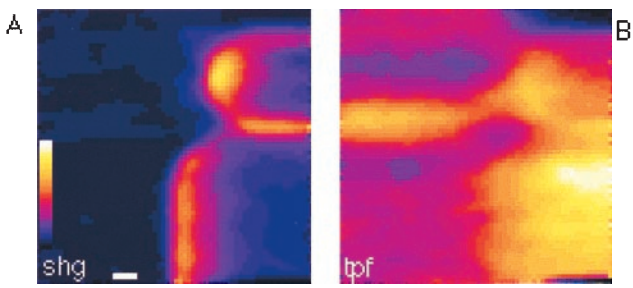


FIG. 2. Second harmonic (*A*) and two-photon (*B*) images of an undifferentiated neuronal cell line. The cells are stained with a membrane probe JPW 1259. The dynamic range is 256 gray levels, and the white scale bar in *A* is 2 microns.

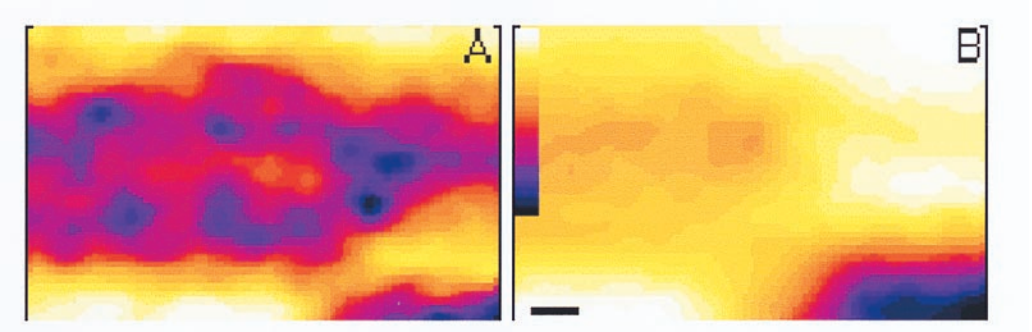


FIG. 3. Second harmonic (*A*) and two-photon (*B*) images of cells of the same cell line as in Fig. 2 stained with the membrane potential probe JPW 1259. However, these cells also were labeled with a 1-nm diameter gold-conjugated antibody. [The contrast here is inverted (black = 256)]. The black scale bar in *B* is 2 microns.

appears as a faint elliptical deep purple halo. These three cells are more evident in the two-photon image because of the internalized dye molecules that also contribute to the signal. The cell in the upper left that is barely visible in the second harmonic image is now clearly defined. This is generally seen in second harmonic imaging when the cells being imaged have their membrane potential depolarized. This results from the sensitivity of the second harmonic generation to cellular membrane potential. According to earlier calibrations that have been performed (2), the cell in the upper left hand portion of the second harmonic image seen in Fig. 2*A* is in a state of nearly complete depolarization.

In Fig. 3 *A* and *B* are seen the effect on the second harmonic and two photon images of 1-nm gold particles that are complexed to goat anti-mouse IgG that is interacting with the primary monoclonal antibody against the carbohydrate antigen, sialyl stage-specific embryonic antigen 1, on the cell membrane. In these images, the 1-nm gold particles are clearly observed tracing the cell membrane in the second harmonic image. However, in the two-photon image, only the internalized dye contributes to the image. Dynamical phenomena induced by the laser during imaging cannot explain this difference between the two-photon and SHG images because we successively imaged the two-photon and second harmonic images and showed no changes in the images over several cycles of recording the frames seen in Fig. 3 *A* and *B*. All of our data point to the reasonable assumption that the gold particles are probably quenching the two-photon fluorescence in the same locations at which they are enhancing the second harmonic signal. In general, the 1-nm gold particles enhance SHG by a factor of ≈2.5 and quench TPF by a factor of 5–10. In other experiments, we also examined larger gold particles (10 and 20 nm). These generally give larger SHG enhancements of a factor of ≈5 but smaller TPF quenching of a factor of 2. It should be noted that these data are highly variable, presumably depending heavily on the molecule–particle distance and on other factors, such as surface densities and relative orientations of the dye molecules and the gold particles as well as other factors yet to be determined. It also should be noted that optimization of these factors could achieve the even larger enhancements predicted by theory (12).

The fact that the dye JPW 1259 has a very large induced dipole can explain both the SHG and TPF observations. The ground state dipole of similar dyes have been estimated by molecular orbital calculations (21, 22) to be ≈10 Debye, and the change in dipole moment between the ground state and the first excited state has been determined by electrochromism measurements (22) to be approximately −16 Debye; rhodamine 6G, a dye often used as a reference for SHG measurements, has a very small dipole by comparison. Although a large induced dipole contributes to the enhancement of the SHG, the same large induced dipole would result in significant quenching of the two-photon fluorescence, and this we have seen both here and in previous studies (18) of single nanoparticles complexed to dye molecules on a glass slide. It is important to note that, when the gold nanoparticle bound membrane was left unstained, no nonlinear signal was detectable. In addition, the presence of the dye alone on the cell membrane results in a second harmonic signal that is considerably weaker than what is obtained in the presence of the gold nanoparticle. Thus, the presence of the dye in the vicinity of a gold ball is essential for the nonlinear optical signal, and the presence of the gold nanoparticle is essential for the enhancement. Therefore, the dipolar interaction of the dye with the nanoparticle seems essential for the observation of enhanced second harmonic generation that is seen in Fig. 3*A*.

Electron microscopic studies of these cells with this 1-nm gold label have provided us with the data that permits us to

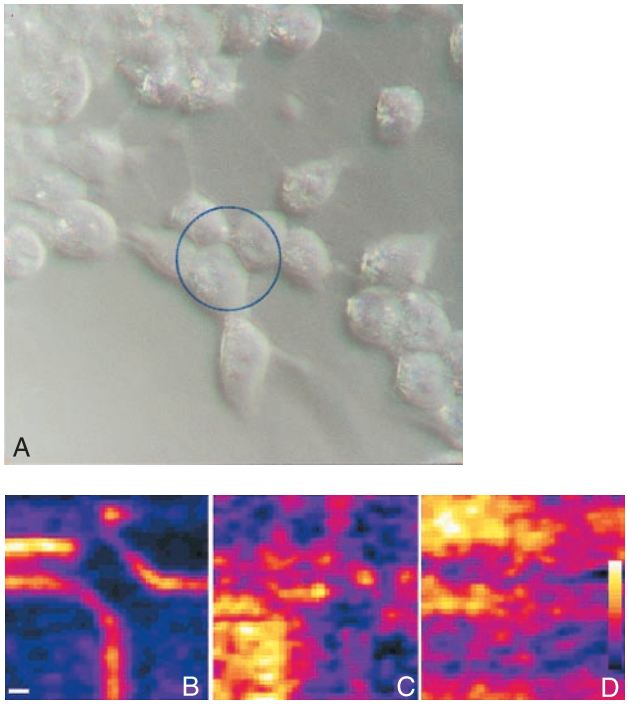


FIG. 4. (*A*) A conventional optical micrograph of a group of cells that are stained with JPW 1259 and are labeled with the 1-nm gold-conjugated antibody. A portion of the field of view that is indicated by a circle in *A* was imaged by using second harmonic generation in (*B*, *C*, and *D*). In *B*, the presence of the nanoparticles on the membranes enhances the second harmonic signal, which traces the membrane outline. Images *C* and *D* were obtained during and after an acidic wash was applied, and this caused a disordering of the 1-nm gold-conjugated antibodies. The scale bar in *B* is 2 microns.

choose the right dilution protocol to achieve a density of gold labeling that matches the *xy* resolution of the optical microscope. These studies also have shown that, on acidic washing of gold-labeled cells, one can disrupt the specific binding of the nanoparticles, and aggregation of the particles is seen. We have observed the same phenomenon in our second harmonic images, and this is seen in Fig. 4. In Fig. 4*A* is the linear optical microscopic image of a group of cells that also are imaged by using second harmonic generation in Fig. 4*B*. In Fig. 4 *C* and *D*, the same cells are imaged by second harmonic generation during and after a gold particle aggregating acidic wash. As can clearly be seen, the result of the acidic wash is to cause significant aggregation of the particles that are bound in an orderly fashion in the membrane in Fig. 4*B*. This further verifies the presence of the nanoparticles in these images. Furthermore, controls were performed to demonstrate that the acidic wash did not cause a depolarization of the cell membrane potential. In addition, two photon-imaging was used simultaneously as a monitor to demonstrate that the morphology of the cells was not changed by the conditions of the acidic wash.

In Fig. 5 *A* and *B* it is shown that the 1-nm gold nanoparticle enhancement of the SHG does not alter the sensitivity of the SHG imaging to membrane potential. As is seen in Fig. 5 *A* and *B*, the depolarization of the cell membrane caused by changing the extracellular KCl concentration from 5.4 to 44.7 mM results in a change of the SHG signal that is qualitatively seen as a reduction in the intensity of the SHG signal of the cell membrane as compared with background. The actual quantitative alteration in the membrane potential as of result of this increase in the KCl concentration was an average reduction of the SHG signal by 59%. The data used to compute this average is seen in Fig. 5*C*. In Fig. 5*C*, the pixel intensities for rows 12–17 in Fig. 5 *A* and *B* are shown as a line of pixels before and after increasing the KCl concentration. The plots indicate that the SHG signal is enhanced in discrete regions and these discrete points of SHG intensity are reduced in magnitude and, in some cases, totally disappear as a result of the depolarization. As can clearly be seen in this figure, the peaks are consistently reduced, with an average value of the reduction summed over all of the peaks being 59%. The relative sensitivity of the enhanced SHG signal to alterations in membrane potential is similar to what we have seen for the dye without nanoparticle enhancement.

The images shown in the figures above represent a detection of single molecule SHG and the optical reporting of the

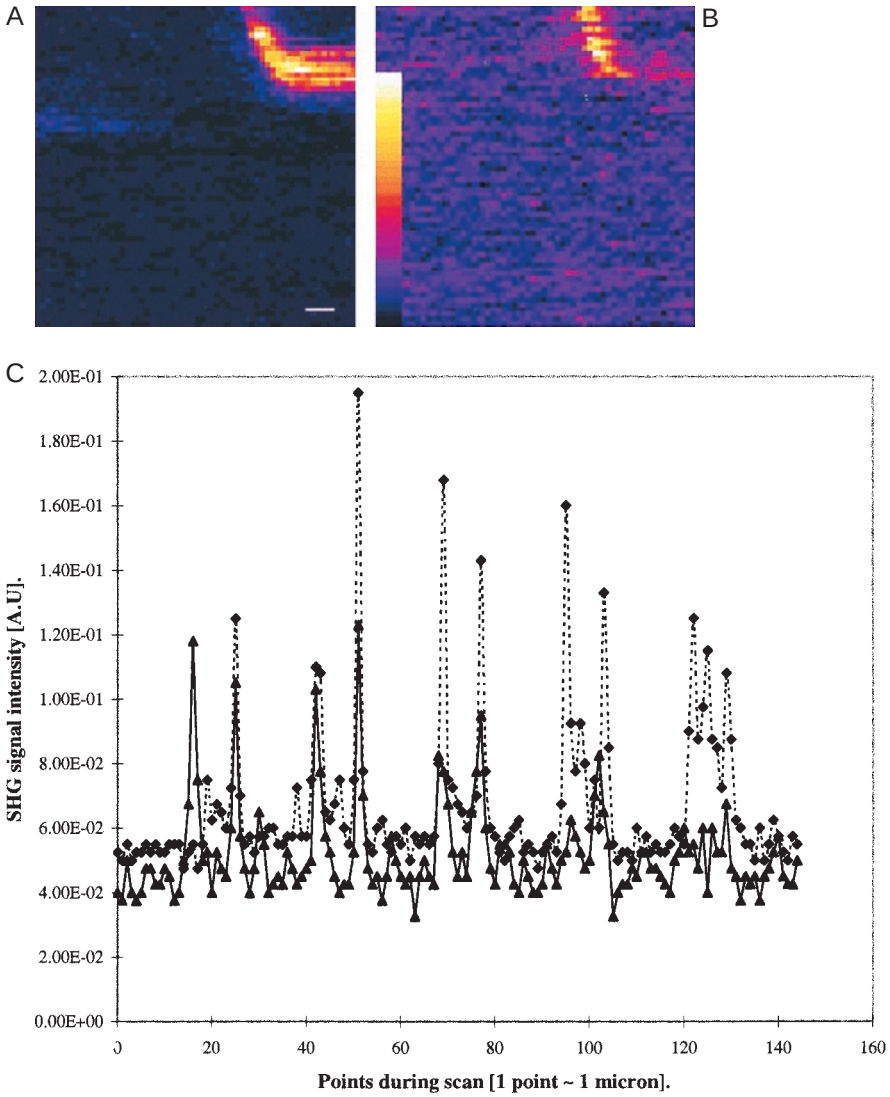


FIG. 5. One-nanometer gold-labeled and JPW 1259-stained cells as in Fig. 3 imaged by second harmonic microscopy before (*A*) and after (*B*) depolarization of the cell membrane. (*C*) To facilitate assessment of the potential dependence of SHG, a plot of intensities taken from a string of pixels in the 64 × 64 images before (dotted line) and after (filled line) membrane depolarization. The pixels chosen for this plot include horizontal rows 12–17 that are plotted in this graph as one continuous line; high-intensity spikes correspond to cell membrane regions near a gold particle.

cellular membrane potential around single molecules. We deduce this from the following computation of how many molecules are enhanced by one particle and the concentration of the label in the cell membrane. An approximate measure of the number of dye molecules that were used to stain the membrane is 1% of the total lipid molecules in the membrane of the cell. This also is assumed to be the concentration in the solution at which the concentration is even less than in the membrane as a result of washing the cells after staining.

For our calculation we focus on the dye molecules in the membrane and assume a radius of a lipid molecule of 3.85 Å. Knowing the concentration of the dye, we can say that one dye molecule is found (on average) every 463.6 $Å^2$. It can be shown that nanoparticles have a very steep dependence of the enhancement of the nonlinear signal on the separation of the molecule from the nanoparticle (data not shown). This arises from the spatial dependence of the dipole–dipole coupling, where, in the nonlinear case, more interacting fields are involved and produce a steeper spatial dependence from what has been calculated for linear phenomena such as spontaneous Raman scattering. Specifically, the nonlinear optical signal is expected to fall off by a factor of $6 \times 10^{-12}$ over a distance of 21 Å. Therefore, a gold nanoparticle of 1-nm diameter enhances effectively a region equal to the area of its equatorial plane. Thus, for a 1-nm gold ball, 0.17 dye molecules are enhanced. This, of course, is a mean value. One caveat to this calculation is the fact that there is some probability, according to the manufacture of the gold-labeled antibodies, that there may be up to three such gold balls on one antibody. However, even if this is the case, the ratio of dye molecules to these three gold particles organized in a way that would give a maximal dimension results in an average of less than one molecule per complex of three particles. In terms of signal enhancement, such a multiple nanoparticle enhancement may shift the plasmon resonance to the near infrared, which could result in further enhancement from important contributions of fields at the fundamental frequency.

In summary, in this paper we achieve functional nonlinear optical imaging of membrane potential in 1-nm regions of cell membranes with single molecule selectivity. Detection of 1-nm gold balls has never been achieved optically and is even very difficult to do in the electron microscope. In addition, we have shown that, with the enhancement in intensity that such nanoparticles afford, we can detect the SHG signal of single dye molecules that are used to stain the cell membrane of a neuronal cell line. These measurements based on SHG are practically zero-background experiments because only those molecules closely associated with the membrane bound nanoparticles give rise to the SHG signal. There is no contribution to the signal from dye molecules that are internalized or dye molecules that are not asymmetrically distributed in the cell membrane. Thus, this opens the door to studies in which a caged neurotransmitter is released with an ultraviolet laser while the membrane potential is being monitored optically in 1-nm regions with an interrogating near-infrared laser. We also expect in the future significant improvement in the observed signal enhancement from such nanoparticles as these particles are optimized in terms of their geometry and in terms of their position relative to the dye-stained cell membrane. With such advancements, we expect that single-channel openings and closings in multiple locations could be dynamically monitored optically with this methodology as a compliment to patch clamping and with the ability to optically monitor, simultaneously, cellular ionic concentrations with two-photon imaging.

We acknowledge the assistance by Hassia Boschwitz with the growing of the cell cultures. We are pleased to thank the Office of Naval Research, United States Navy, for a grant in support of this work. Partial support from the U.S. Public Health Service is also gratefully acknowledged. A.L acknowledges the support from The US-Israel Binational Science Foundation and The Ministry of Science and Technology (Israel). G.P. received a Levi Eshkol doctoral fellowship from the Ministry of Science and Technology (Israel).

1. Bouevitch, O., Lewis, A., Ben-Oren, I., Wuskell, J. & Loew, L. (1993) *Biophys. J.* **65,** 672–679.
2. Ben-Oren, I., Peleg, G., Lewis, A., Minke, B. & Loew L. (1996) *Biophys. J.* **71,** 1616–1620.
3. Nie S. & Zare R. N. (1997) *Annu. Rev. Biophys. Biomol. Struct.* **26,** 567–596.
4. Denk, W., Strickler, J. H. & Webb, W. W. (1990) *Science* **248,** 73–76.
5. Hell, S. W., Schrader, M. & Van Der Voort, H. T. M. (1997) *J. Microsc.* **187,** 1–7.
6. Berland, K. M., So, P. T. C. & Gratton, E. (1995) *Biophys. J.* **68,** 694–701.
7. Svoboda, K. D., Tank, D. W. & Denk, W. (1996) *Science* **272,** 716–719.
8. Svoboda, K., Denk, W., Kleinfeld, D. & Tank, D. W. (1997) *Nature (London)* **385,** 161–165.
9. Kerker, M., Wang, D. S., Chew, H., Siiman, O. & Bumm, L. A. (1982) in *Surface Enhanced Raman Scattering*, eds. Chang, R. K. & Furtak, T. E. (Plenum, New York), pp. 109–128.
10. Boyd, G. T., Rasing, T., Leite, R. R. & Shen, Y. R. (1984) *Phys. Rev. B.* **30,** 519–526.
11. Chen, C., Heinz, T. F., Ricard, D. & Shen, Y. R. (1981) *Phys. Rev. Lett.* **46,** 1010–1012.
12. Wessel, J. (1985) *J. Opt. Soc. Am. B* **2,** 1538–1541.
13. Huang, J. Y., Chen, Z. & Lewis, A. (1989) *J. Phys. Chem.* **93,** 3314–3320.
14. Huang, J. Y., Lewis, A. & Loew, L. (1988) *Biophys. J.* **53,** 665–670.
15. Chen, Z., Sheves, M., Lewis, A. & Bouevich, O. (1994) *Biophys. J.* **67,** 1155–1160.
16. Bouevitch, O., Lewis, A. & Sheves, M. (1995) *J. Phys. Chem.* **99,** 10648–10657.
17. Levine, J. M. & Flynn, P. (1986) *J. Neurosci.* **6,** 3374–3384.
18. Peleg, G., Lewis, A., Bouevitch, O., Loew, L., Parnas, D. & Linial, M. (1996) *BioImaging* **4,** 215- 224.
19. Tsuyuoka, K., Yago, K., Hirashima, K., Ando, S., Hanai, N., Saito, H., Yamasaki, K. M., Takahashi, K., Fukuda. Y., Nakao, K., *et al.* (1996) *J. Immunol.* **157,** 661–669.
20. Sorkin, A., Eriksson, A., Heldin, C. H., Westermark, B. & Claesson-Welsh, L. (1993) *J. Cell. Physiol.* **156,** 373–382.
21. Loew, L. M., Bonneville, G. W. & Surow, J. (1978) *Biochemistry* **17,** 4065–4071.
22. Loew, L. M. & Simpson. L. (1981) *Biophys. J.* **34,** 353–365.